JOURNAL OF SOLID STATE CHEMISTRY 78, 52–65 (1989)

Phase Transitions and Structural Relationships between Ge_5F_{12}, GeF_2, SnF_2, and TeO_2

GEORGES DENES

Department of Chemistry, Laboratories for Inorganic Materials, Laboratory of Solid State Chemistry and Mössbauer Spectroscopy, Concordia University, 1455 De Maisonneuve Boulevard West, Montreal, Quebec, Canada H3G 1M8

Received February 1, 1988; in revised form August 8, 1988

Oxidation of 20% of Ge(II) to Ge(IV) in GeF_2 leads to Ge_5F_{12}, whose chain structure with GeF_6 weak interchain bridges, is closely related to the chain structure of GeF_2 with weak interchain fluorine bridges. Results reported in the literature about a monoclinic high-temperature phase of GeF_2 are reexamined in the light of crystallographic and crystal chemistry considerations, which lead to the conclusion that the high-temperature cell is most likely erroneous. It is shown that GeF_2 most likely undergoes a ferro- to paraelastic $\beta \rightleftharpoons \gamma$ transition similar to the β-$SnF_2 \rightleftharpoons \gamma$-$SnF_2$ and high-pressure $TeO_2 \rightleftharpoons$ paratellurite TeO_2 transitions. High-temperature GeF_2 is probably tetragonal like γ-SnF_2 and TeO_2 and its powder pattern contains, in addition, weak peaks of Ge_5F_{12} and/or SiO_2, due to hydrolysis of a minor part of the sample by moisture.

Introduction

Stannous fluoride SnF_2 is known to exist in three different crystalline phases, namely α, β, and γ (*1*). α-SnF_2, the stable phase at room temperature, crystallizes from H_2O/HF solutions in the monoclinic $C2/c$ space group. It contains two kinds of tin(II) atoms, Sn(1) in a pseudotetrahedral SnF_3E coordination and Sn(2) in a pseudooctahedral SnF_5E coordination, where E is the tin(II) electron lone pair (*2*). The two kinds of tin are linked together by fluorine bridges to form Sn_4F_8 tetramers. Upon heating to 150–190°C, depending on grain size (*1, 3*), the γ-phase is obtained. γ-SnF_2 crystallizes in the tetragonal space group $P4_12_12$ or $P4_32_12$, with tin(II) being in a SnF_4E trigonal bipyramid (*4, 5*). Upon cooling, at 66°C, γ-SnF_2 undergoes a second-order displacive transition, giving orthorhombic ferroelastic β-SnF_2 (space group $P2_12_12_1$) (*1*), which contains one kind of tin(II) in a distorted $SnF_4F'E$ coordination intermediate between a trigonal bipyramid and an octahedron (*4, 5*).

GeF_2 crystallizes in the orthorhombic $P2_12_12_1$ space group and is isostructural to β-SnF_2 and high-pressure TeO_2 (*6, 7*). Ge(II) is coordinated by three fluorine atoms and a lone pair (E), forming GeF_3E pseudotetrahedra, linked together by weak interactions, while three-dimensional networks are observed in β- and γ-SnF_2. There is one report in the literature on the existence of a high-temperature form of GeF_2, which was found to be monoclinic (*8*). The preparation of a mixed oxidation state fluo-

0022-4596/89 $3.00

ride of germanium, Ge_4F_{10}, better written as $Ge_3^{II}Ge^{IV}F_{10}$, has been published (*9*); however, its crystal structure shows that it is Ge_5F_{12}, i.e., $Ge_4^{II}Ge^{IV}F_{12}$, instead of Ge_4F_{10} (*10*). Mixed oxidation state fluorides of tin have also been reported, viz. Sn_7F_{16}, Sn_3F_8, Sn_2F_6, and $Sn_{10}F_{34}$ (*11*), but the crystal structure of Sn_3F_8 only is known (*12*), and they will not be discussed further here.

Stannous fluoride SnF_2 is stable in air at room temperature, except for a minor surface oxidation of the particles (*13*). Therefore, it can be easily studied and requires special precautions only at high temperature, when it should be held in a dry inert atmosphere to prevent hydrolysis to black SnO by moisture and oxidation to stannic tin by oxygen (*1*). On the other hand, GeF_2 is highly sensitive to air, as it is very hygroscopic, even deliquescent, resulting in orange germanous hydroxide being produced (*6, 8–10, 14*). This makes the study of GeF_2 much more delicate than that of SnF_2. High-temperature studies are extremely difficult and hydrolysis in silica capillary tubes with attack of the glass have been reported (*8*). In contrast, Ge_5F_{12}, thought to be Ge_4F_{10} at the time, has been reported to be much less hygroscopic, and as a result, to be a convenient storage chemical for GeF_2 and GeF_4, which are both extremely hygroscopic and are both obtained upon thermal decomposition of Ge_5F_{12} (*3*).

We present here striking analogies between the crystal structures of GeF_2 and Ge_5F_{12} on one hand and GeF_2, SnF_2, and TeO_2 on the other hand, which have not been reported before. The interrelationships between these structures led us to an analysis of the phase transition reported to take place for GeF_2 at 62°C. Analogies with the transition of TeO_2 at 9 kbar are also presented. The structural effect of the oxidation of 20% of Ge(II) in GeF_2 to Ge(IV), to give Ge_5F_{12}, is shown. Orthorhombic GeF_2 is referred to as β-GeF_2 hereafter because it is isotypic with β-SnF_2. In light of the structural interrelationships mentioned above, it is concluded that the high-temperature phase of GeF_2 is tetragonal, similar to that of γ-SnF_2 and paratellurite TeO_2, instead of monoclinic as reported in the literature.

Analogies between the Crystal Structures of GeF_2 and Ge_5F_{12}

1. Molecular Volume

The crystal structure of compounds with a stereoactive lone pair of electrons is usually highly distorted due to low symmetry at the central atom site (lone pair carrier), resulting in highly anisotropic structures. These are usually well interpreted in terms of bonding pair–nonbonding pair (lone pair) repulsions within the first sphere of coordination and between the first and second spheres of coordination (*15–17*). Galy *et al.* (*16*) showed that the volume occupied by the lone pair is equivalent to that of a fluorine or an oxygen atom in Te(IV) compounds. Denes *et al.* (*2, 4*) showed that this is also true for Sn(II) compounds. Although crystallographic data on germanium oxides/fluorides are much more scarce, Table I shows that the above is also valid for Ge(II)-containing structures, as, with the exception of monoclinic GeF_2, the V_2 molecular volume per anion, with the Ge(II) lone pair being counted as an anion, is fairly constant, regardless of the oxidation state of germanium. Table I also shows that the Ge(II) lone pair is stereoactive in orthorhombic GeF_2 and Ge_5F_{12}. The data for monoclinic GeF_2 will be discussed in the paragraph on the analogies between the crystal structures and phase transitions of GeF_2, SnF_2, and TeO_2.

2. Unit-Cell Relationships

The unit-cell parameters for orthorhombic β-GeF_2 and Ge_5F_{12} are given in Table II. As shown in Fig. 1, the monoclinic cell of

TABLE I

COMPARISON OF THE VOLUME PER ANION FOR Ge(II)- AND Ge(IV)-CONTAINING FLUORIDES AND OXIDES

Compounds	Crystal system	V (Å^3)[a]	Z[b]	V_1 (Å^3)[c]	V_2 (Å^3)[d]	References[e]
β-GeF_2[f]	Orthorhombic	201.51	4	25.19	16.79	(6)
GeF_2	Monoclinic	283.55	4	35.44	23.63	(8), TW
GeF_2	Monoclinic	283.55	5	28.36	18.90	(8), TW
GeF_2	Monoclinic	283.55	6	23.63	15.75	(8), TW
γ-GeF_2	Tetragonal	202.05	4	25.26	16.84	TW
Ge_5F_{12}	Monoclinic	515.57	2	21.48	16.11	(10)
GeO_2	Tetragonal	55.33	2	13.83	13.83	(18)
GeO_2	Hexagonal	121.73	g	g	g	(19)

[a] Volume of the unit cell.
[b] Number of molecules in the unit cell.
[c] Molecular volume per anion (anions = F and/or O).
[d] Molecular volume per anion (anions = F and/or O + E), counting the Ge(II) lone pair E as an anion.
[e] TW = this work.
[f] Orthorhombic GeF_2 is called here β-GeF_2, because it is isostructural with β-SnF_2 (4).
[g] As Z is not reported in (19), V_1 and V_2 could not be determined.

Ge_5F_{12} is a bidimensional supercell of the orthorhombic cell of β-GeF_2. The matrix of transformation is

$$\begin{vmatrix}\mathbf{a}\\ \mathbf{b}\\ \mathbf{c}\end{vmatrix}_{Ge_5F_{12}} = \begin{vmatrix}\frac{1}{2} & \frac{3}{2} & 0\\ \frac{3}{2} & -\frac{1}{2} & 0\\ 0 & 0 & 1\end{vmatrix} \cdot \begin{vmatrix}\mathbf{a}\\ \mathbf{b}\\ \mathbf{c}\end{vmatrix}_{\beta\text{-}GeF_2} \quad (1)$$

The result is that the relationship between the volumes is $V(Ge_5F_{12}) = 5V(\beta\text{-}GeF_2)/2$.

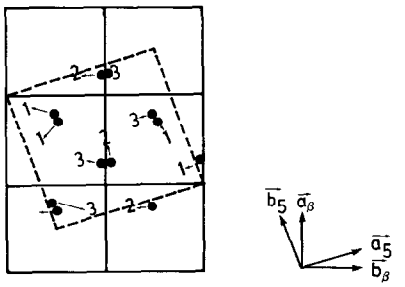

FIG. 1. Monoclinic cell of Ge_5F_{12} as a superlattice of the orthorhombic cell of β-GeF_2. Solid circles are Ge(II) atoms in β-GeF_2. Numbers 1 to 3 are Ge atoms in Ge_5F_{12} according to the numbering in (10). Arrows indicate the shift of Ge atoms from GeF_2 to Ge_5F_{12}. Subscripts "β" and "5" refer to β-GeF_2 and Ge_5F_{12}, respectively.

This is in agreement with the molecular formula $(GeF_2) \times 5/2 = Ge_5F_{10}$, the two extra fluorine atoms resulting from the oxidation of 20% of Ge(II) to Ge(IV). As shown in Table II, the unit-cell parameters of the supercell (right-hand side column) are close to the observed values. The higher volume

TABLE II

COMPARISON OF THE OBSERVED AND CALCULATED UNIT CELLS OF Ge_5F_{12} WITH THAT OF β-GeF_2

	$(\beta\text{-}GeF_2)_o$[a]	$(Ge_5F_{12})_o$[a]	$(Ge_5F_{12})_c$[b]
a (Å)	4.682	8.356	8.312
b (Å)	5.178	7.590	7.486
c (Å)	8.312	7.969	8.112
β (°)	90	93.03	90.00
V (Å^3)	205.51	516.30	504.76
Z	4	2	2
Crystal system	Orthorhombic	Monoclinic	Monoclinic
Space group	$P2_12_12_1$	$P2_1/c$[c]	$P2_1/c$
Reference	(6)	(10)	TW[d]

[a] Observed values.
[b] Calculated values, as a supercell of β-GeF_2.
[c] The structure of Ge_5F_{12} presented in (10) is described in the nonconventional space group $P2_1/a$. In this paper, all values have been converted to the conventional $P2_1/c$ space group (No. 14).
[d] TW = this work.

(2.4%) can be accounted for by the two extra fluorine atoms, although it is partly cancelled by the disappearance of the lone pair of 20% of the Ge(II) atoms, and maybe also by a more efficient packing. It is clear from these results that oxidation of one-fifth of the divalent germanium of β-GeF_2 to give Ge_5F_{12} is, from a structural point of view, mostly a bidimensional phenomenon.

3. *Structural Relationships*

The structure of β-GeF_2 contains a pseudotetragonal pseudobody-centered sublattice of Ge similar to that observed in rutile-type GeO_2. The cationic sublattice is close to that of GeO_2, whereas comparison of Figs. 2a and 2b shows that the anion sublattice is much more perturbed, probably because of the fluorine lone pair repulsions. The doubling of the c axis of β-GeF_2 relative to that of GeO_2 results from the deviation from exact centering of Ge. A similar analogy of β-SnF_2 to SnO_2 was previously reported by us (*4*). The structure of

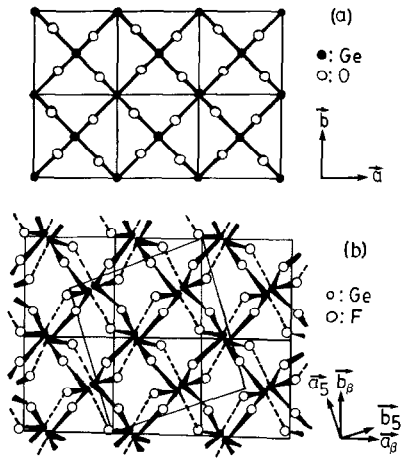

FIG. 2. Comparison of the structures of GeO_2 and β-GeF_2: (a) rutile-type GeO_2 with a tetragonal body-centered sublattice of Ge, octahedrally coordinated by oxygen; (b) distortion of the rutile lattice in β-GeF_2, with the c parameter being doubled. The dashed lines show longer Ge–F interactions. The supercell of Ge_5F_{12} is shown.

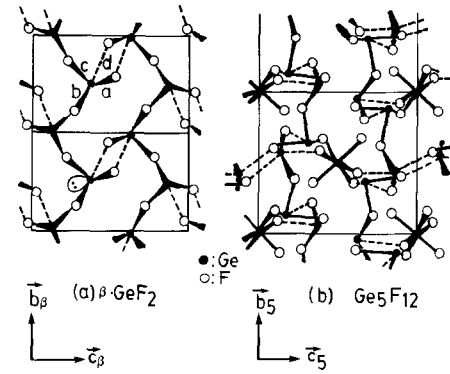

FIG. 3. Comparison between the structures of β-GeF_2 and Ge_5F_{12}. Weak interactions are shown by dashed lines. (a) Chain structure of β-GeF_2 with weak interchain bridges. Ge–F distances are a = 1.788 Å, b = 1.909 Å, c = 2.094 Å, and d = 2.570 Å. (b) Pseudochain structure of Ge_5F_{12} with weakly bridging Ge(IV)F_6 distorted octahedra.

β-GeF_2 consists of zigzag chains of GeF_2 molecules linked by strong fluorine bridges along the **b** axis, with weaker bridges along **a**, making it essentially a chain structure (Fig. 3a).

In Ge_5F_{12}, the structure is more complex. As shown in Fig. 3b, a system of Ge(II)–F chains is still found parallel to the **b** axis; however, the bridges between each Ge_2F_4 group, within each chain, are weaker. In addition, in Ge_5F_{12}, the three-dimensional cohesion of the structure is due to weak bridges to the equatorial fluorines of the Ge(IV)F_6 distorted octahedra, the two axial fluorines of the octahedron being terminal.

The transition from β-GeF_2 to Ge_5F_{12} upon oxidation of 20% of Ge(II) to Ge(IV) can be understood in terms of adding two fluorine atoms on Ge(2) to give a Ge(IV)F_6 distorted octahedron, with simultaneous motion of Ge(1)F_2 and Ge(3)F_2 groups, to form a new stable structure. The motion of the GeF_2 group, shown by arrows in Fig. 1, conserves the GeF_2 groups, except for Ge(2), which is oxidized to a Ge(IV)F_6^{2-} octahedron, and involves mostly a rearrangement of the lengths and angles of bridges.

TABLE III

UNIT-CELL PARAMETERS AND ATOMIC COORDINATES FOR ORTHORHOMBIC β-GeF_2, β-SnF_2, AND HP-TeO_2 AT ROOM TEMPERATURE

		β-GeF_2[a]	β-SnF_2	HP-TeO_2[b]
a (Å)		4.682(1)	4.9889(7)	4.6053(6)
b (Å)		5.178(1)	5.1392(6)	4.8557(6)
c (Å)		8.312(1)	8.4777(14)	7.5300(10)
Ge/Sn/Te	x	0.266(4)	0.274(5)	0.274(2)
	y	0.008(5)	0.023(7)	0.012(2)
	z	0.131(3)	0.130(5)	0.117(2)
F(1)/O(1)	x	0.528(24)	0.541(6)	0.549(2)
	y	0.082(24)	0.163(5)	0.120(2)
	z	0.982(18)	0.996(3)	0.940(1)
F(2)/O(2)	x	0.433(18)	0.378(4)	0.406(2)
	y	0.246(29)	0.202(2)	0.234(2)
	z	0.279(18)	0.385(4)	0.333(1)
References		(6)	(4)	(7)

[a] There are eight possible positions for the origin of the cell in $P2_12_12_1$. The structure of β-GeF_2 was solved using a different origin than β-SnF_2 and TeO_2. All results in this table are given using the same origin after the following transformation: $(x, y, z)_{GeF_2} = (\frac{1}{2} - x, y, z)_{TeO_2/SnF_2}$.

[b] At 19.8 kbar.

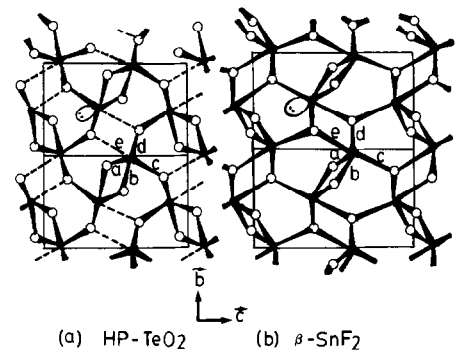

FIG. 4. Comparison between the structures of (a) HP-TeO_2 (Te–O distances are a = 1.912 Å, b = 2.034 Å, c = 2.044 Å, d = 2.110 Å, and e = 2.586 Å) and (b) β-SnF_2 (Sn–F distances are a = 1.89 Å, b = 2.26 Å, c = 2.40 Å, d = 2.41 Å, e = 2.49 Å).

Analogies between the Crystal Structures and Phase Transitions of GeF_2, SnF_2, and TeO_2

1. Crystal Structures of β-GeF_2, β-SnF_2, and High-Pressure TeO_2

β-GeF_2, β-SnF_2, and high-pressure TeO_2 (HP-TeO_2) crystallize in the $P2_12_12_1$ orthorhombic space group with similar unit-cell parameters and atomic coordinates (*4*, *6*, *7*), as shown in Table III. In all three cases, the cationic sublattice is pseudobody-centered, similar to that found in the rutile type (Fig. 2a). However, departure from the ideal body-centered lattice is shown in Fig. 2b by the lack of cations distant from $c/2$ in superimposing exactly on the projection parallel to **c**, which results in a doubling of the c parameter relative to rutile. Figure 2b also shows that the anionic sublattice is even more distorted compared to rutile (Fig. 2a). Figures 3a and 4 also show the pseudobody-centered sublattice of cations in β-GeF_2, HP-TeO_2, and β-SnF_2.

Examination of Table IV shows that, despite their similar cells and atomic coordinates, the metal coordination is not the same in the three isotypic structures of β-GeF_2, HP-TeO_2, and β-SnF_2. Indeed, germanium in β-GeF_2 has a threefold coordination, with one short bond to a terminal fluorine and two longer bonds to bridging fluorines, which results in a chain structure, as shown in Fig. 3a. Weaker interactions between the terminal fluorines of one chain and the germaniums of neighboring chains

TABLE IV

THE SIX SHORTEST METAL–ANION DISTANCES IN ISOTYPIC β-GeF_2, HP-TeO_2, AND β-SnF_2

d_{M-X} (Å)	β-GeF_2	HP-TeO_2	β-SnF_2
1	1.79	1.912	1.89
2	1.91	2.034	2.26
3	2.09	2.044	2.40
4	2.57	2.110	2.41
5	3.26	2.586	2.49
6	3.34	2.922	3.79

provide sufficient cohesion to keep the compound in the solid state. For HP-TeO_2 (Fig. 4a), the tellurium coordination is 4, the weaker interaction observed in β-GeF_2 being much stronger and thus able to make a real oxygen bridge in HP-TeO_2. In addition, a fifth interaction, much weaker, is also observed. As a result, this is a three-dimensional structure. In β-SnF_2 (Fig. 4b), tin is in a fivefold coordination similar to the tellurium coordination in HP-TeO_2, but with the fifth weak interaction of HP-TeO_2 being now strong enough to be a bridging bond. This is also a three-dimensional structure. The increase of coordination number from Ge(II) to Te(IV) and to Sn(II) is in agreement with increasing ionic radii: Ge^{2+}, 0.736 Å; Te^{4+}, 0.976 Å; Sn^{2+}, 1.228 Å (*20*).

The coordination of Ge(II), Te(IV), and Sn(II) is governed by their size and electronic structure. All three have the same electronic structure, [Kr] $4d^{10}5s^25p^0$, with one lone pair of electrons nonengaged in bonding. However, this lone pair is hybridized: (i) sp^3 in Ge(II), resulting in a pseudotetrahedral GeF_3E coordination, (ii) sp^3d in Te(IV), giving a pseudotrigonal bipyramidal TeO_4E polyhedron, and (iii) sp^3d^2 in Sn(II), resulting in a distorted SnF_5E octahedron. In each case, one corner of the polyhedron is occupied by the lone pair E (*16*), and the polyhedron is highly distorted by the strong lone pair–bonding pair repulsions (*15*).

The bonding scheme and weaker interactions can be explained using the bond valence method of Brown (*17*), considering the various ways a regular octahedron can be distorted by a lone pair located on the central atom (Fig. 5). A lone pair along a threefold axis gives a distorted MX_3E tetrahedron; along a twofold axis, a MX_4E trigonal bipyramid; and along a fourfold axis, a distorted MX_5E octahedron, called by Brown $\mathscr{C}$, $\mathscr{A}$, and $\mathscr{E}$ models, respectively. However, often the lone pair is not located

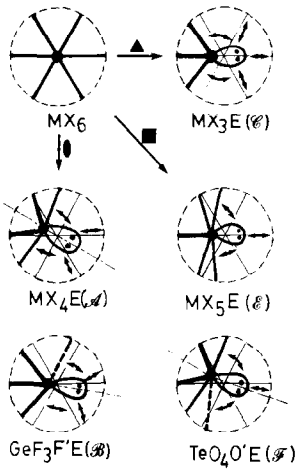

FIG. 5. Distortion of a regular octahedron by a lone pair of electrons along a rotation axis as defined by Brown (*17*). Model $\mathscr{F}$, as reported for HP-TeO_2, was hitherto unreported. Lone pair–bonding pair repulsions are shown by ↷ ; and lone pair–other atoms repulsions by ↔.

along a rotation axis, and further distortion is observed as the polyhedron has no axial symmetry. This is the case of β-SnF_2, with a distorted SnF_5E octahedron (distorted $\mathscr{E}$ model). In some cases, when the lone pair is located between two rotation axes, additional weaker interactions occur, such as the $GeF_3F'E$ polyhedron around Ge(II) in β-GeF_2, with three short bonds (although unequal), and a fourth weaker interaction. This is the $\mathscr{B}$ model of Brown, which is intermediate between a MX_3E tetrahedron and a MX_4E trigonal bipyramid. The $TeO_4O'E$ polyhedron in HP-TeO_2, with four strong bonds and a weaker interaction, is intermediate between a MX_4E trigonal bipyramid and a MX_5E octahedron. This model was not given by Brown (*17*), probably because no such geometry had so far been reported. We have represented it in Fig. 5 and called it $\mathscr{F}$. The lone pair–bonding pair repulsions, larger than the repulsions between bonding pairs, in agreement with the VSEPR model (*15*), are responsible for the closing of X–M–X angles and are

shown by curved double arrows (↷) in Fig. 5. The repulsions between the lone pair and the other atoms shown by straight double arrows (↔) are responsible for the smaller coordination numbers and apparent voids in the structures, which, in fact, are occupied by the lone pairs.

As stated earlier, a lone pair occupies a volume similar to that of a fluorine or an oxygen atom. Therefore, the molecular volume per anion V_2 (see Table I) should be similar for GeF_2 and GeO_2 on one hand and SnF_2 and SnO_2 on the other hand. Table I and the work of Denes *et al.* (*2, 4*) shows that this is the case. Discrepancies are due to packing efficiency of anions around the central cation (which is a function of the coordination number) and packing of polyhedra in the solid. Table V shows that V_2 for β-SnF_2 is 1.17% larger than that of SnO_2, whereas the value for β-GeF_2 is 21.40% larger than for GeO_2. This indicates that the fivefold coordination of Sn(II) in β-SnF_2 and the three-dimensional polymeric network of Sn–F bonds provides a packing almost as efficient as in rutile-type SnO_2. On the other hand, packing in β-GeF_2 is much more inefficient. This is probably due to the lower coordination number of Ge and to the pseudounidimensionality of this chain structure. The less dense packing of β-GeF_2 is also shown by the percentage difference between the V_2 values of β-SnF_2 and GeF_2 of 7.87%, much lower than the 66.85% value predicted from the ionic radii of Sn^{2+} and Ge^{2+}, whereas the value of 29.50% for SnO_2 and GeO_2 is very close to the theoretical value of 30.19% obtained from the ionic radii of Sn^{4+} and Ge^{4+}. The larger metal–lone pair distance for Ge(II) [Ge(II)–E = 1.05 Å] than for Sn(II) [Sn(II)–E = 0.95 Å] (*16*) most likely results in more dead space in the β-GeF_2 structure, and, therefore, further decreases packing efficiency.

TABLE V

COMPARISON OF THE PERCENTAGE DIFFERENCE IN VOLUME PER ANION FOR MF_2 AND MO_2 (M = Ge AND Sn)

$100 \times [V_2(\beta\text{-}SnF_2) - V_2(SnO_2)]/V_2(SnO_2) =$	1.17%
$100 \times [V_2(\beta\text{-}GeF_2) - V_2(GeO_2)]/V_2(GeO_2) =$	21.40%
$100 \times [R(Sn^{4+}) - R(Ge^{4+})]/R(Ge^{4+}) =$	30.19%
$100 \times [V_2(SnO_2) - V_2(GeO_2)]/V_2(GeO_2) =$	29.50%
$100 \times [R(Sn^{2+}) - R(Ge^{2+})]/R(Ge^{2+}) =$	66.85%
$100 \times [V_2(\beta\text{-}SnF_2) - V_2(\beta\text{-}GeF_2)]/V_2(\beta\text{-}GeF_2) =$	7.87%

Note. The volumes of SnO_2 and GeO_2 (rutile form) are taken from the data of Ref. (*21*). The ionic radii of Sn^{4+} and Ge^{4+}, in coordination 6, were taken from Ref. (*20*). The data for β-SnF_2 were taken from Ref. (*4*). β-GeF_2 refers to orthorhombic GeF_2 (*6*), as in Table I.

TABLE VI

CALCULATED DENSITY VERSUS NUMBER OF MOLECULES IN THE UNIT CELL FOR m-GeF_2

	Z	ρ_c (g cm^{-3})	$\Delta\rho/\rho$ (%)[a]
β-GeF_2[b]	4	3.644	—
m-GeF_2	4	2.59	−29.04
	5	3.22	−11.78
	6	3.88	+ 6.30

[a] $\Delta\rho/\rho$ (%) = percentage density change at the β-$GeF_2 \rightarrow$ m-GeF_2 phase transition.

[b] Values taken from (*6*).

2. *The Monoclinic Cell of GeF_2 at High-Temperature (m-GeF_2)*

Hereafter, the high-temperature monoclinic phase of GeF_2 is referred to as m-GeF_2. Adams *et al.* (*8*) reported a phase transition in GeF_2 at 62°C, with H°_{trans} = −0.11 kcal mol^{-1}; therefore, this is a first-order transition. The powder pattern of the high-temperature phase was indexed in monoclinic with a = 4.87 Å, b = 8.58 Å, c = 7.55 Å, β = 116° (we have changed the nonconventional cell of (*8*) to a conventional monoclinic cell with **b** as unique axis).

Using the volume of 283.5 Å^3 for the cell of m-GeF_2, one can determine its calculated density (ρ_c) for given assumptions on the value of the number of molecules in the unit cell (Z). The results in Table VI show

that no value of Z is likely to explain the β-$GeF_2 \rightarrow$ m-GeF_2 transition satisfactorily. $Z = 4$ results in a 29% decrease in compactness; such a high value is highly unlikely except for some transformations from high-pressure phases to ambient pressure phases. $Z = 5$ gives an 11.8% decrease in density. This is a reasonable value; however, it would be highly unlikely to have five molecules in the unit cell as this results in at least two different types of Ge (there is no site of multiplicity 5 in any monoclinic space group), and, therefore, the high-temperature phase would be more highly ordered than the low-temperature phase, a very unlikely situation. $Z = 6$ would result in a more highly packed and more highly ordered phase at high temperature than at room temperature, which are two highly unlikely situations.

Although automatic indexation using the procedure of Ito (*22*) is usually reliable and provides a reasonable indexation of the power pattern of GeF_2 at high temperature, the study of density changes shows that the monoclinic cell proposed in (*8*) is not adequate, as it would result in unlikely changes in packing. In addition, it is very rare to find a high-temperature phase of lower symmetry and more order than the room-temperature phase of the same compound.

3. New Propositions for the Modification of GeF_2 at High Temperature

The search for alternate explanations for the thermal and X-ray pattern changes of GeF_2 at high temperature are based (i) on the very high reactivity of GeF_2 and its sensitivity to traces of moisture, and (ii) on the structural analogies between GeF_2, SnF_2, and TeO_2. Even if the work in (*8*) was done carefully, it is difficult to be certain that no hydrolysis occurred. Two possibile reactions have been considered.

a. Partial hydrolysis giving a mixture of Ge_5F_{12} and GeO_2. According to the reaction

$$6GeF_2 + 2H_2O \rightarrow Ge_5F_{12} + GeO_2 + 2H_2 \quad (1)$$

one-sixth of the total GeF_2 is hydrolyzed by traces of moisture, giving GeO_2 and Ge_5F_{12}. The X-ray powder pattern of Ge_5F_{12} has not been published; however, it can be calculated from the unit cell given in (*10*). It is clear from the results of Table VII that the whole pattern of m-GeF_2 can be indexed in the monoclinic cell of Ge_5F_{12}. Moreover, the agreement between observed and calculated d spacings is better; as for the m-GeF_2 cell, the average $|d_o - d_c|/d_o$ value is 0.51% with six values larger than 1%, the highest being 3.70%. On the other hand, for the Ge_5F_{12} cell, the average value is 0.23%, only three are larger than 1%, and the highest value of 2.64% occurs for the first peak, i.e., at low θ angle, in a region where the d values are less accurate. To the contrary, in the m-GeF_2 cell, the largest value of 3.70% is found at a larger θ angle for the 10th observed peak. These results support well the hypothesis that Ge_5F_{12} could be the main component of high-temperature GeF_2. GeO_2 could be present as an amorphous or microcrystalline phase or in the rutile form. For the rutile-type phase, the (110), (200), and (211) peaks calculated from the data of (*21*) should occur at 3.1077, 2.1975, and 1.6197 Å, respectively, which agrees well with the peaks observed at 3.123, 2.191, and 1.630 Å, respectively.

b. Phase transition giving tetragonal γ-GeF_2, and partial hydrolysis producing HF, which attacks the silica capillary tubes. As shown above, orthorhombic β-GeF_2 is isotypic with β-SnF_2 and HP-TeO_2. The orthorhombic distortion of β-SnF_2 disappears at 66°C, giving tetragonal γ-SnF_2. Similarly, paratellurite TeO_2 is tetragonal at ambient pressure, and isotypic with γ-SnF_2. From these analogies, one can postulate that, at high temperature, GeF_2 gives a tetragonal form γ-GeF_2, isotypic to γ-SnF_2 and TeO_2. A good approximation of the

TABLE VII

COMPARISON OF THE INDEXATION OF THE POWDER PATTERN OF THE HIGH-TEMPERATURE PHASE OF GeF_2 IN THE m-GeF_2 MONOCLINIC CELL (*8*) AND IN THE MONOCLINIC CELL OF Ge_5F_{12} (*10*)

m-GeF_2[a]				Ge_5F_{12}[b]		
h k l	d_o (Å)	d_c (Å)	Δd (%)	*h k l*	d_c (Å)	Δd (%)
1 0 0	4.285	4.3739	2.07	2 0 0	4.172	2.64
0 2 0		4.2895	0.11			
1 1 0	4.008	3.8967	2.78	0 0 2	3.979	0.72
0 0 2	3.429	3.3952	0.99	0 2 1	3.425	0.12
1 1 2	3.310	3.2691	1.24	1 1 2	3.302	0.24
1 2 1	3.194	3.1816	0.39	1 2 1	3.194	0.00
				1 1 2	3.193	0.03
0 1 2	3.123	3.1569	−1.09	1 2 1	3.144	−0.67
1 0 1		3.1087	0.46			
0 2 2	2.672	2.6622	0.37	2 2 1	2.677	−0.19
0 3 1	2.606	2.6355	1.13	2 2 1	2.618	−0.46
				3 1 0	2.612	−0.23
2 0 1	2.416	2.4131	0.12	1 3 0	2.421	−0.21
				0 3 1	2.411	0.21
0 0 3	2.279	2.3634	3.70	1 3 1	2.306	−1.18
				2 2 2	2.256	1.01
1 0 2	2.227	2.2470	−0.90	3 1 2	2.235	−0.36
				3 0 2	2.225	0.09
0 3 2	2.191	2.1872	0.17	2 1 3	2.196	0.23
2 0 0		2.1870	0.18	3 2 1	2.184	0.32
0 4 0	2.144	2.1448	−0.04	3 2 1	2.136	0.37
				3 1 2	2.135	0.42
				0 3 2	2.135	0.42
0 2 3	1.987	2.0018	0.74	3 2 2	1.991	−0.20
1 2 2		1.9904	−0.17	0 0 4	1.989	−0.10
2 2 0	1.939	1.9484	−0.48	4 1 1	1.927	0.62
1 4 0		1.9257	0.69	0 1 4	1.924	0.77
1 0 4	1.877	1.8858	−0.47	3 3 0	1.872	0.27
2 1 1	1.818	1.8155	0.14	3 1 3	1.816	0.11
0 4 2		1.8132	0.26			
1 0 3	1.717	1.7251	−0.47	3 3 2	1.717	0.00
0 5 0		1.7158	0.07	2 1 4	1.714	0.17
				0 4 2	1.713	0.23
0 1 4	1.658	1.6653	−0.44	3 0 4	1.660	−0.12
0 5 1		1.6635	−0.33			
3 0 2	1.630	1.6221	0.48	4 2 2	1.633	−0.18
				5 1 0	1.630	0.00
1 5 1	1.613	1.6135	−0.03	5 1 1	1.613	0.00
				4 3 0	1.610	0.19
1 2 3	1.595	1.6005	−0.34	2 2 4	1.597	−0.13
				2 4 2	1.597	−0.13
				4 3 1	1.590	0.31
0 4 3	1.561	1.5568	0.27	0 3 4	1.564	−0.19
2 0 2		1.5543	0.43	0 1 5	1.558	0.19
2 2 2	1.459	1.4614	−0.16	2 4 3	1.462	0.21
3 0 0		1.4580	0.07	1 2 5	1.458	0.07
				3 2 4	1.458	0.07

TABLE VII—*Continued*

m-GeF_2[a]				Ge_5F_{12}[b]		
h k l	d_o (Å)	d_c (Å)	Δd (%)	*h k l*	d_c (Å)	Δd (%)
3 1 0	1.434	1.4374	−0.24	2 1 5	1.435	−0.07
				1 2 5	1.434	0.00
				2 4 3	1.433	0.07
3 2 0	1.381	1.3804	0.04	5 3 1	1.383	−0.14
				4 1 4	1.380	0.07
				4 2 4	1.378	0.22
0 5 3	1.364	1.3673	−0.24	6 1 0	1.368	0.30
2 3 2		1.3657	−0.12	6 1 1	1.360	0.29
				2 2 5	1.364	0.00
				1 4 4	1.363	0.07
1 4 3	1.341	1.3442	−0.24	3 3 4	1.340	0.07
0 1 5		1.3414	−0.03	1 3 5	1.339	0.15
				4 4 2	1.339	0.15
1 2 4	1.319	1.3226	−0.27	1 0 6	1.321	−0.15
				1 3 5	1.321	−0.15
				3 5 1	1.320	−0.08
				2 4 4	1.319	0.00
				0 5 3	1.318	0.08
3 3 0	1.298	1.2989	−0.07	1 0 6	1.299	−0.08
0 2 5		1.2947	0.25	6 2 1	1.299	−0.08
				5 2 3	1.297	0.08
				5 3 2	1.297	0.08
				1 5 3	1.296	0.15
2 5 1	1.258	1.2604	−0.19	4 4 3	1.259	−0.08
2 4 2		1.2586	−0.05	6 2 2	1.259	−0.08
0 5 4	1.209	1.2068	0.25	2 6 0	1.211	−0.17
				5 4 2	1.209	0.00
				0 5 4	1.207	0.17
				3 1 6	1.207	0.17
				4 5 1	1.207	0.17
3 5 2	1.182	1.787	0.28	5 2 4	1.184	−0.17
				2 2 6	1.183	−0.08
				2 4 5	1.183	−0.08
				4 5 2	1.183	−0.08
				5 4 2	1.182	0.00
$\Sigma\lvert\Delta d\rvert/N(hkl)$[c]: m-$GeF_2$ = 0.51%						
Ge_5F_{12} = 0.23%						

[a] Data taken from (*8*) for monoclinic GeF_2 (m-GeF_2), after transformation to the standard monoclinic system with **b** as unique axis.

[b] Calculated using the cell in (*10*), after transformation to the standard $P2_1/c$ space group, as given in Table II.

[c] $\Delta d = ((d_o - d_c)/d_o) \times 100$. $N(hkl)$ = number of (hkl) families of planes indexed.

unit cell of the hypothetic γ-GeF_2 can be obtained by analogy with the $\beta \rightarrow \gamma$ transition of SnF_2, and used for indexing its powder pattern. In addition, hydrolysis of a part of GeF_2 would most likely produce HF, which would attack the SiO_2 capillary tubes, producing SiF_4 vapor, which would hydrolyze back to SiO_2. We previously ob-

served (*23*) that such mechanisms produce various varieties of silica. The data of Table VIII show that the powder pattern of GeF_2 at high temperature can be successfully indexed as a mixture of tetragonal GeF_2 and SiO_2 in α-quartz, α-cristobalite, and α-tridymite forms. The average relative difference between observed and calculated d_{hkl}

TABLE VIII

COMPARISON OF THE INDEXATION OF THE POWDER PATTERN OF THE HIGH-TEMPERATURE PHASE OF GeF_2 IN THE m-GeF_2 MONOCLINIC CELL (δ) AND IN A MIXTURE OF TETRAGONAL γ-GeF_2 AND SiO_2

m-GeF_2[a]					γ-GeF_2 or SiO_2[b]			
I_{obs}	$h\ k\ l$	d_o (Å)	d_c (Å)	Δd (%)	I_γ	$(hkl)_\gamma/SiO_2$[c]	d_c (Å)	Δd (%)
vw	1 0 0	4.285	4.3739	−2.07		Q	4.260	0.58
	0 2 0		4.2895	−0.11				
mw	1 1 0	4.008	3.8967	2.78		C	4.040	−0.80
						T	4.002	0.15
S	0 0 2	3.429	3.3952	0.99	S	1 1 0	3.434	−0.09
S	1 1 2	3.310	3.2691	1.24	VS	1 0 2	3.214	2.90
w	1 2 1	3.194	3.1816	0.39		T	3.229	1.10
						C	3.162	1.00
S	0 1 2	3.123	3.1569	−1.09		C	3.138	−0.48
	1 0 1		3.1087	0.46				
w	0 2 2	2.672	2.6622	0.37		1 1 2	2.680	−0.30
m	0 3 1	2.606	2.6355	1.13	w	T	2.591	0.58
w	2 0 1	2.416	2.4131	0.12	m	2 0 0	2.427	−0.46
w	0 0 3	2.279	2.3634	3.70	vw	2 0 1	2.335	−2.46
						T	2.286	−0.31
vw	1 0 2	2.227	2.2470	−0.90	vw	1 1 3	2.197	1.35
w	0 3 2	2.191	2.1872	0.17	vw	2 1 0	2.170	0.96
	2 0 0		2.1870	0.18				
vw	0 4 0	2.144	2.1448	−0.04	w	0 0 4	2.145	−0.05
mS	0 2 3	1.987	2.0018	0.74	vw	1 0 4	1.962	1.26
	1 2 2		1.9904	−0.17				
w	2 2 0	1.939	1.9484	−0.48	S	2 1 2	1.937	0.10
	1 4 0		1.9257	0.69				
mS	1 0 4	1.877	1.8858	−0.47	vw	2 0 3	1.850	1.44
						C, T	1.870	0.37
mS	2 1 1	1.818	1.8155	0.14	m	1 1 4	1.819	−0.06
			1.8132	0.26				
m	1 0 3	1.717	1.7251	−0.47		2 2 0	1.716	0.06
	0 5 0		1.7158	0.07				
	0 1 4	1.658	1.6653	−0.44		Q	1.659	−0.06
mw	0 5 1		1.6635	0.33				
mw	3 0 2	1.630	1.6221	0.48	m	1 0 5	1.618	0.74
mw	1 2 3	1.595	1.6005	−0.34		2 0 4	1.607	−0.75
mS	0 4 3	1.561	1.5568	0.27		3 1 0	1.532	1.86
	2 0 2		1.5543	0.43				

$\Sigma|\Delta d|/N(hkl)$[d]: m-GeF_2 = 0.69
γ-GeF_2 or SiO_2 = 0.78

[a,b,d] As in Table VII.
[c] Q = α-quartz, C = α-cristobalite, T = α-tridymite.

is only slightly larger than for the m-GeF_2 cell and the largest discrepancy is smaller (2.90 for tetragonal GeF_2, 3.70 for m-GeF_2). In addition, the peak intensity pattern for tetragonal GeF_2, hereafter called γ-GeF_2 by analogy with isotypic γ-SnF_2, is similar to that of γ-SnF_2, as expected. Except for one, all peaks for SiO_2 are weak, therefore, due to minor contamination.

4. Orthorhombic → Tetragonal Phase Transitions of GeF_2, SnF_2, and TeO_2

The isotypic orthorhombic phases of β-GeF_2, β-SnF_2, and HP-TeO_2 belong to the $P2_12_12_1$ space group, which can exhibit the property of "ferroelasticity"; i.e., the crystals are subject to an internal spontaneous strain, which usually results in multidomain crystals. Existence of ferroelastic behavior has been proved in β-SnF_2 and HP-TeO_2, using the techniques of X-ray and neutron powder diffractions (*4, 5, 7, 24*). These compounds undergo a phase transition from ferroelastic to paraelastic properties, upon heating, at 66°C for SnF_2, and upon reducing pressure, at 9 kbar for TeO_2. In both cases, the phase transition is a second-order displacive one, such that the tetragonal space group of the paraelastic phase is a supergroup of $P2_12_12_1$, in agreement with Landau's theory of second-order transitions (*25*), and as tabulated by Ascher (*26*) and Aizu (*27*). Both paraelastic γ-SnF_2 and TeO_2 crystallize in $P4_12_12$ or its enantiomorph $P4_32_12$. As β-GeF_2 is isotypic to HP-TeO_2 and β-SnF_2, one could expect it to experience a similar type of phase transition upon heating, giving a high-temperature tetragonal phase of GeF_2 that we call γ-GeF_2 by analogy with γ-SnF_2. The likelihood of such transition taking place in GeF_2 is reinforced by the two following observations:

(i) All strong diffraction peaks of HT-GeF_2 can be indexed in a tetragonal cell similar to that of γ-SnF_2, as shown in Table VIII. In addition, the similar pattern of line intensities suggest that γ-SnF_2 and γ-GeF_2 are isotypic. The weak lines can be explained by hydrolysis of a part of the sample, giving SiO_2 and/or Ge_5F_{12}.

(ii) The following mathematical relationships between the unit-cell parameters of β-GeF_2 and m-GeF_2 suggest that the cell of m-GeF_2 is a superstructure of that of β-GeF_2.

$$a_m \approx (a_\beta + b_\beta)/2 \tag{2}$$

$$b_m \approx c_\beta \tag{3}$$

$$c_m \approx [(3a_\beta/2)^2 + (3b_\beta/4)^2]^{1/2} \tag{4}$$

$$\beta \approx 90° + \text{arc sin}[(3a_m/4)/c_m], \tag{5}$$

where a_m, b_m, c_m, β, and a_β, b_β, c_β are the unit-cell parameters of m-GeF_2 and β-GeF_2, respectively.

The tetragonal unit cell for γ-GeF_2, obtained from the indexation of Table VIII, is comparable to the cells of isotypic γ-SnF_2 and paratellurite TeO_2 (Table IX). Contrary to the monoclinic cell, it requires no drastic change of density. It follows that the β-GeF_2 cell is an orthorhombic distortion of the γ-GeF_2 cell, and that the m-GeF_2 cell is a superstructure of that of γ-GeF_2, the two cells being related as follows:

$$\begin{vmatrix}\mathbf{a}\\ \mathbf{b}\\ \mathbf{c}\end{vmatrix}_\gamma = \begin{vmatrix}1 & 0 & 0\\ \frac{1}{2} & 0 & \frac{2}{3}\\ 0 & 1 & 0\end{vmatrix} \begin{vmatrix}\mathbf{a}\\ \mathbf{b}\\ \mathbf{c}\end{vmatrix}_m \tag{6}$$

$$V_\gamma = 2V_m/3. \tag{7}$$

The relationship between the monoclinic and the tetragonal cells of HT-GeF_2 is shown in Fig. 6.

As stated above, the ferro- to paraelastic transitions of TeO_2 and SnO_2 are second-order transition; i.e., they do not involve any latent heat and volume change at the transition point. However, the first derivatives of these parameters, i.e., the heat capacity and thermal expansion coefficients (versus T) or hydrostatic compressibility

TABLE IX

UNIT CELL OF PARAELASTIC PARATELLURITE TeO_2, γ-SnF_2, AND γ-GeF_2

	TeO_2	γ-SnF_2	γ-GeF_2
a (Å)	4.8052	5.072	4.853
c (Å)	7.6021	8.493	8.579
V (Å^3)	175.53	218.48	202.05
Z	4	4	4
ρ_c (g cm^{-3})	6.04	4.76	3.64
T (°C)	20	80	80
Space group	$P4_12_12$ or $P4_32_12$	$P4_12_12$ or $P4_32_12$	$P4_12_12$ or $P4_32_12$?
Reference	(7)	(28)	TW[a]

[a] TW = this work.

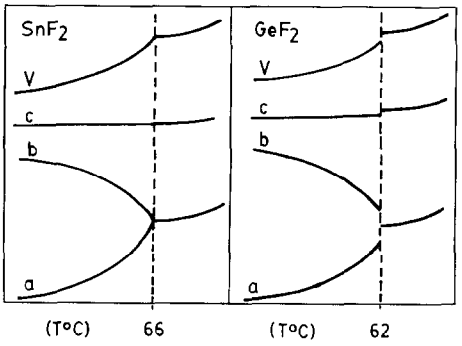

FIG. 7. Unit cell parameters and volume versus temperature, as observed for $\beta \rightleftharpoons \gamma$-$SnF_2$, and as suggested for $\beta \rightleftharpoons \gamma$-$GeF_2$. (Scales are in arbitrary units.)

coefficients (versus P), can undergo drastic changes, and this has been shown to be the case for the expansion coefficients of SnF_2 (*1*, *5*, *28*) and TeO_2 (*7*, *24*). However, a DTA study of GeF_2 has shown that the transition at 62°C is associated with an enthalpy of -0.11 kcal mol^{-1}. Therefore, this is a first-order transition. As a consequence, there is no subgroup–supergroup requirement for the space group of γ-GeF_2 as for TeO_2 and γ-SnF_2. Thus, in principle γ-GeF_2 need not crystallize in the $P4_12_12$ or $P4_32_12$ space group. However, of course, it can, and the indexation of Table VIII and the similar intensity of Bragg peaks suggest that it does. It is well known that a phase transition that is of second order at a given pressure can be of first order at another pressure. Therefore, there is no contradiction in the fact that the $\beta \rightleftharpoons \gamma$-$SnF_2$ transition is a second-order one and the $\beta \rightleftharpoons \gamma$-$GeF_2$ a first-order one. In addition, the reversibility of the $\beta \rightleftharpoons \gamma$-$GeF_2$ transition, not required for first-order transitions, suggests that it can be second order at another pressure and that it requires no drastic structural change. Therefore, it is probably displacive, like the transition of SnF_2. Most likely, a sudden change of unit-cell parameters and volume occurs at the transition, of the type suggested in the model of Fig. 7.

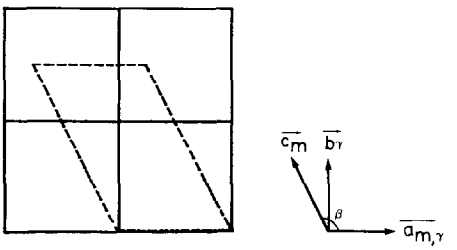

FIG. 6. γ-GeF_2 tetragonal cell and m-GeF_2 supercell.

Conclusion

The crystal structures of Ge_5F_{12}, GeF_2, SnF_2, and TeO_2 are closely related. The unit cell of Ge_5F_{12} is a supercell of that of β-GeF_2. The chain structure of β-GeF_2, with weak interchain links through secondary interactions, changes to a similar chain structure with weakly bridging GeF_6 units between the $(GeF_2)_n$ chains, upon oxidation of 20% of Ge(II) to Ge(IV).

The data reported for the high-temperature phase of GeF_2 have been reanalyzed. Based on crystallographic considerations and the structural relationships quoted above, it is concluded that the monoclinic cell reported in the literature is a supercell of the real cell, which is most likely tetragonal, isotypic to γ-SnF_2 and TeO_2 paratellurite. The powder pattern of HT-GeF_2 can

be successfully indexed in the monoclinic cell of Ge_5F_{12} or in a tetragonal γ-GeF_2 cell with SiO_2 impurity lines, which could be due to hydrolysis of a part of the sample by traces of moisture. The tetragonal γ-GeF_2 cell, similar to that of γ-SnF_2 and TeO_2, accounts well for molecular volume considerations (Table I) and number of molecules in the unit cell (Table VI), contrary to the monoclinic supercell. In addition, it fits a model of ferro- to paraelastic phase transitions which is observed in SnF_2 and TeO_2.

Upon heating GeF_2 in the experiment of (*8*), hydrolysis of a part of the sample probably occurred, resulting in some Ge_5F_{12} and/or SiO_2 being produced. This does not contradict the reversibility reported in (*8*), as the weak peaks of Ge_5F_{12} may be difficult to see at room temperature because of overlapping with the peaks of γ-GeF_2, which is probably responsible for the line broadening reported in (*8*). The reversibility observed in (*8*) was probably the reversible first-order transition $\beta \rightleftharpoons \gamma$-$GeF_2$, all strong peaks of HT-GeF_2 being concerned by this transition.

A study of GeF_2 versus temperature, by X-ray diffraction on a single crystal or by neutron diffraction on powder, would be most appropriate to study the atomic displacement as a function of temperature in order to confirm the proposed ferroelastic properties.

Acknowledgments

Concordia University and the Programme d'Actions Structurantes of Quebec are gratefully acknowledged for financial support. The Natural Science and Engineering Research Council of Canada is thanked for a University Research Fellowship.

References

1. G. DENES, *Mater. Res. Bull.* **15,** 807 (1980).
2. G. DENES, J. PANNETIER, J. LUCAS, AND J. Y. LE MAROUILLE, *J. Solid State Chem.* **30,** 335 (1979).
3. G. DENES, *J. Solid State Chem.* **37,** 16 (1981).
4. G. DENES, J. PANNETIER, AND J. LUCAS, *J. Solid State Chem.* **33,** 1 (1980).
5. J. PANNETIER, G. DENES, M. DURAND, AND J. L. BUEVOZ, *J. Physique* **41,** 1019 (1980).
6. J. TROTTER, M. AKHTAR, AND N. BARTLETT, *J. Chem. Soc. A,* 30 (1966).
7. T. G. WORLTON AND R. A. BEYERLEIN, *Phys. Rev. B* **12,** 1899 (1975).
8. G. P. ADAMS, L. M. ALBRITTON, D. W. BONNELL, J. L. MARGRAVE, J. SCOTT, AND P. W. WILSON, *J. Less-Common Met.* **24,** 113 (1971).
9. G. P. ADAMS, J. L. MARGRAVE, AND P. W. WILSON, *J. Inorg. Nucl. Chem.* **33,** 1301 (1971).
10. J. C. TAYLOR AND P. W. WILSON, *J. Amer. Chem. Soc.* **95,** 1834 (1973).
11. R. SABATIER, A. M. HEBRARD, AND J. C. COUSSEINS, *C.R. Acad. Sci. Paris Ser. C* **279,** 1121 (1974).
12. M. F. A. DOVE, R. KING, AND T. J. KING, *J. Chem. Soc., Chem. Commun.,* 944 (1973).
13. T. BIRCHALL, G. DENES, K. RUEBENBAUER, AND J. PANNETIER, *J. Chem. Soc., Dalton Trans.,* 1831 (1981).
14. N. BARTLETT AND K. C. YU, *Canad. J. Chem.* **39,** 80 (1961).
15. R. J. GILLESPIE AND R. S. NYHOLM, *Q. Rev. Chem. Soc.* **11,** 339 (1957).
16. J. GALY, G. MEUNIER, S. ANDERSSON, AND A. ÅSTRÖM, *J. Solid State Chem.* **13,** 142 (1975).
17. I. D. BROWN, *J. Solid State Chem.* **11,** 214 (1974).
18. Natl. Bur. Standards Circ. **539,** 8 (1958).
19. SWANSON AND TATGE, J.C. Fel. Reports, NBS (1950); ASTM 4-097; W. H. ZACHARIASEN, *Z. Kristallogr.* **67,** 226 (1928).
20. R. D. SHANNON, *Acta Crystallogr. Sect. A* **32,** 751 (1976).
21. A. R. WEST, "Solid State Chemistry and Its Applications," p. 225, Wiley, New York (1984).
22. T. ITO, "X-Ray Studies on Polymorphism," Appendix VII, Maruzen Co. Ltd., Tokyo (1950).
23. G. DENES, unpublished results.
24. E. F. SKELTON, J. L. FELDMAN, C. Y. LIU, AND I. L. SPAIN, *Phys. Rev. B* **13,** 2605 (1976).
25. L. LANDAU AND E. LIFCHITZ, "Statistical Physics," MIR Editions, Moscow (1967).
26. E. ASCHER, "Lattices of Equi-Translation Subgroups of the Space Groups," Battelle Institute, Advanced Studies Center, Geneve (1968).
27. K. AIZU, *Phys. Rev. B* **2,** 754 (1970).
28. G. DENES, *J. Solid State Chem.* **36,** 20 (1981).